Fluorometric virus detection platform using quantum dots-gold nanocomposites optimizing the linker length variation

Fluorometric virus detection platform using quantum dots-gold nanocomposites optimizing the linker length variation

Fahmida Nasrin,[a,†] Ankan Dutta Chowdhury,[b,†] Kenshin Takemura,[a] Ikko Kozaki,[c] Hiroyuki Honda,[c] Oluwasesan Adegoke[b,‡], Enoch Y. Park[*,a,b]

[a]*Laboratory of Biotechnology, Graduate School of Science and Technology, Shizuoka University, 836 Ohya, Suruga-ku, Shizuoka 422-8529, Japan*

[b]*Laboratory of Biotechnology, Research Institute of Green Science and Technology, Shizuoka University, 836 Ohya, Suruga-ku, Shizuoka 422-8529, Japan*

[c]*Department of Biomolecular Engineering, Graduate School of Engineering, Nagoya University, Furo-cho, Chikusa-ku, Nagoya 464-8603, Japan*

[†] Equally contributed.

[‡] Present address: Leverhulme Research Centre for Forensic Science, University of Dundee, UK

E-mails:
fahmida.nasrin.17@shizuoka.ac.jp (FN)
ankan.dutta.chowdhury@shizuoka.ac.jp (ADC)
takemura.kenshin.16@shizuoka.ac.jp (KT)
kozaki.ikkou@b.mbox.nagoya-u.ac.jp (IK)
honda@chembio.nagoya-u.ac.jp (HH)
o.adegoke@dundee.ac.uk (OA)
park.enoch@shizuoka.ac.jp (EYP)

[*]Corresponding Author at Research Institute of Green Science and Technology, Shizuoka University, 836 Ohya Suruga-ku, Shizuoka 422-8529, Japan.
E-mail addresses: park.enoch@shizuoka.ac.jp (E.Y. Park)

ABSTRACT:

In this study, a tunable biosensor using the localized surface plasmon resonance (LSPR), controlling the distance between fluorescent CdZnSeS/ZnSeS quantum dots (QDs) and gold nanoparticles (AuNPs) has been developed for the detection of virus. The distance between the AuNPs and QDs has been controlled by a linkage with a peptide chain of 18 amino acids. In the optimized condition, the fluorescent properties of the QDs have been enhanced due to the surface plasmon effect of the adjacent AuNPs. Successive virus binding on the peptide chain induces steric hindrance on the LSPR behavior and the fluorescence of QDs has been quenched. After analyzing all the possible aspect of the CdZnSeS/ZnSeS QD-peptide-AuNP nanocomposites, we have detected different concentration of influenza virus in a linear range of 10^{-14} to 10^{-9} g mL^{-1} with detection limit of 17.02 fg mL^{-1}. On the basis of the obtained results, this proposed biosensor can be a good alternative for the detection of infectious viruses in the various range of sensing application.

Keywords: Biosensor; Gold nanoparticle; Influenza virus; Localized surface plasmon resonance; Peptide; Quantum dots.

1. Introduction

For the development of biosensor, numerous promising approaches have been introduced in the last two decades to use the surface and interfacial properties of different nanostructure materials by achieving an appropriate combination [1-4]. In particular, noble-metal nanoparticles such as gold nanoparticles (AuNPs) have been studied extensively because of their chemical stability, versatility and unique optical properties such as localized surface plasmon resonance (LSPR), which lead to the enhancement of a wide variety of local and nanoscale optical fields [5-9]. As an extension of these proposed methods, fluorescent inorganic quantum dots (QDs) have been widely used in LSPR-based biosensor in which the fluorescence signal is directly influenced by the adjacent AuNPs depending on various size, shape and distance [8, 10-12]. Due to the easy fabrication process, drastic changes in fluorescence intensities, rapidity, requiring low number of samples and low detection limits, the LSPR-based biosensor has been emerging significantly [13-16]. However, as these methods are very sensitive, a tiny change in the nanoparticle's formation affects largely on the detection pathways which sometimes restricts its applicability in respect of reliability. Therefore, more investigations are required to optimize the working condition for the establishment of its repeatability. In conventional LSPR-based system, the background of the sensor shows quite high signal due to the initially emitted fluorescent intensity of QDs, causing decrease of sensitivity [17]. As an advancement of the conventional LSPR-based system, an optimized system can be established where the small changes in structural conformation can be used to analyze very low dimensional samples like viruses. In that case, the initial high fluorescence signal should be quenched gradually depending on the analyte concentration. This quenching system can offer higher sensitivity due to the maximum fluorescent enhancement between two rigid nanoparticles with LSPR effect which gradually decreases with increasing concentration

of the hindrance analytes. The structural formation can be tuned by the known distance of linker through peptide chain.

In this report, we have constructed a biosensor system with a nanoconjugate using functionalized CdZnSeS/ZnSeS QDs as a fluorescent probe and AuNPs as an adjacent surface plasmon molecule [18, 19]. In our previous study on norovirus detection, similar system has been already introduced with a crosslinker of 11-mercaptoundecanoic acid to make a rigid sensor [20]. Although the detection limit was quite impressive, however, being a small crosslinker between two nanoparticles, the sensor could not able to signify small changes of virus concentration, precisely. Therefore, to make the sensor more spacious for analyte molecule, an 18 amino acid-based peptide has been used as a linker molecule between these two nanoparticles (Scheme 1). Additionally, the tunable distance between QDs and AuNPs helps to understand the mechanism of the LSPR interaction which can be applied for the sensing. The synthesized peptide has been modified accordingly to anchor the AuNPs and QDs in its both ends to build a stable sensor structure of CdZnSeS/ZnSeS QD-peptide-AuNP. Two aspartic acid residues have been introduced in the used peptide chain for the purpose of antibody binding. To achieve the optimized condition for sensing operation, different sizes and concentrations of AuNPs have been tested on the similar sensor system. In addition, varying the linker distance between QDs and AuNPs using different length of peptide chains has been also investigated. In the optimized condition, the fluorescence of the CdZnSeS/ZnSeS QD-peptide-AuNP has been increased to its maximum. Then the successive detection of different concentration of viruses has been monitored by the quenching of the sensor intensity. The mechanism of detection involves the quenching of the QDs fluorescence due to the restriction of the LSPR signal of AuNPs towards the QDs as illustrated in Scheme 1. To establish the mechanism, influenza virus has been chosen here for the analysis as it is one of the causative agents for the infectious diseases in the respiratory tract which remains as a potential threat for

human healthcare [21-23]. The linearity and detectability have been established in femtomolar to nanomolar range which indicates the potential possibility of this detection method for the virus surveillance in near future.

2. Experimental section

2.1. Materials

Acetone, polyoxyethylene, sulfuric acid (H_2SO_4), sorbitan monolaurate (Tween 20), hydrogen peroxide (H_2O_2), methanol, sodium citrate, potassium hydroxide (KOH), chloroform, tri-sodium citrate ($Na_3C_6H_5O_7$) and phosphate-buffered saline were purchased from Wako Pure Chemical Ind. Ltd. (Osaka, Japan). *N*-(3-dimethylaminopropyl)-*N*-ethylcarbodiimide hydrochloride (EDC), *N*-hydroxysuccinimide (NHS), $HAuCl_4$, bovine serum albumin (BSA), cadmium oxide (CdO), thioglycolic acid (TGA), hexadecylamine (HDA), zinc oxide (ZnO), trioctylphosphine oxide (TOPO), 1-octadecene (ODE), trioctylphosphine (TOP), selenium (Se) and sulfur (S) were purchased from Sigma Aldrich Co., LLC (Saint Louis, MO, USA). Tetramethylbenzidine (TMBZ) was purchased from Dojindo (Kumamoto, Japan). Oleic acid (OA) was purchased from Nacalai Tesque Inc. (Kyoto, Japan).

Primary antibodies against hemagglutinin (HA) proteins of influenza virus A/H1N1 (New Caledonia/20/99) and a mouse monoclonal antibody [B219M], anti-white spot syndrome virus VP28 antibody [AB26935] were purchased from Abcam Inc. (Cambridge, UK). Goat anti-rabbit IgG-horseradish peroxidase (HRP) was purchased from Santa Cruz Biotechnology (CA, USA). Anti-hepatitis E virus (HEV) antibody was kindly provided by Dr. Tian-Cheng Li of Department of Virology, National Institute of Infectious Diseases. Recombinant influenza virus A/H1N1 (New Caledonia/20/99) were purchased from Prospec-Tany Techno Gene Ltd.

(Rehovot, Israel). Norovirus-like particle (NoV-LP) preparation was followed by previous protocol [24]. For selectivity test, Zika virus, HEV-like particle (HEV-LP) and white spot syndrome virus (WSSV) were kindly provided by Professor K. Morita of Institute of Tropical Medicine Nagasaki University, Dr. Tian-Cheng Li of National Institute of Infectious Diseases and Dr. Jun Satoh of National Research Institute of Aquaculture of Japan Fisheries Research and Education Agency, respectively.

2.2. Synthesis and solubilization of CdZnSeS/ZnSeS QDs

Basic precursors such as CdO, ZnO, HDA, ODE, TOP, OA, Se, S were used to carry out the organometallic hot-injection synthesis of CdZnSeS/ZnSeS QDs according to previously reported procedure [25].

KOH-methanolic-TGA solution was used to prepare the water soluble QDs by a ligand exchange reaction [18]. Briefly, 2 mL of TGA was added with 3 g of KOH which was dissolved in 40 mL of methanol and the solution was stirred. Then, hydrophobic QDs solution were added into the KOH-methanolic-TGA solution. The solutions were effectively separated from organic phase to water-soluble phase by stirring for 1 h and thereafter left to stand for overnight. Acetone and chloroform were used to wash QDs by centrifugation. High yield purified water-soluble QDs were obtained through drying in a fume hood.

2.3. Preparation of AuNPs seed and Synthesis of AuNPs growth

For the synthesis of various sized AuNPs, reduction of $HAuCl_4$ was carried out at pH 6.2–6.5 by dissolving Na_3Ctr at 100°C [26]. In brief, 100 mL of 1 mM $HAuCl_4$ was mixed with 200 μL of 1 M NaOH in a 250 mL flask. The solution was boiled and stirred with a magnetic

143 stir-bar. Then, 10 mL of 38.8 mM Na_3Ctr was added rapidly. The reaction was continued until
144 the solution turned into wine-red color. The reflux system was shut down after 15 min of
145 reaction and finally deionized water was added to the solution to make the final volume of
146 ~100 mL.

147 To synthesize AuNPs growth solution, a variable volume of seed solution was added with
148 227 µL of 44.7 mM $HAuCl_4 \cdot 3H_2O$. Later, 176 µL of 38.8 mM $Na_3Ctr \cdot 2H_2O$ was added to the
149 solution with continuous stirring until the color changes from colorless to wine red [26].

150

151 *2.4. Synthesis of sensing probe*

152 Initially, the peptide, which has amine group in one hand and thiol group in another hand,
153 was covalently conjugated with the free carboxylic group of TGA-capped CdZnSeS/ZnSeS
154 QDs by EDC/NHS chemistry [18]. After that, AuNPs were conjugated to another end of
155 peptide where thiol group is present and synthesized the QD-peptide-AuNP nanocomposite.
156 Then, anti-HA antibody (Ab) against influenza virus A/H1N1 was covalently linked with the
157 free carboxyl group of peptides via EDC/NHS reaction. The conjugate mixture was stirred for
158 2–3 h at 7°C to form the sensing probe (QD-peptide-AuNP) which is AuNPs and QDs linked
159 by antibody-conjugated peptide and were purified by using centrifuge for 5 min at 3000 g and
160 eventually dissolved in 2 mL of ultrapure water. A set of 6 nanocomposites with different
161 peptide length (4 to 34 amino acids) has been synthesized for the optimization of the sensor
162 probe where each of the peptide contains two carboxylic acid groups of aspartic acid (D) for
163 the antibody binding. The structures of six peptides are given in **Table S1** of Supplementary
164 data.

165

166 *2.5. Physicochemical analysis*

167 Morphology of surface and size were checked by the images obtained from transmission
168 electron microscopy (TEM) using a TEM (JEM-2100F, JEOL, Ltd., Tokyo, Japan) at 100 kV.
169 An Al Kα X-ray source (1486.6 eV) and a hemispherical electron analyzer was used to carry
170 out X-ray photoelectron spectroscopy (XPS, ESCA1600 system, ULVAC-PHI Inc.). Dynamic
171 light scattering (DLS) was measured by using a Zetasizer Nano series (Malvern Inst. Ltd.,
172 Malvern, UK). Fluorescence emission and UV-Vis absorption measurements were obtained by
173 using a filter-based multimode microplate reader (Infinite F500, TECAN, Ltd, Männedorf,
174 Switzerland). Analysis of Energy dispersive spectroscopy (EDS) was carried out using a
175 scanning electron microscopy system (JEM-16036, JEOL, Ltd., Tokyo, Japan) combined with
176 JED-2300 EDS. Confirmation of antibody conjugation to the QD-peptide-AuNP
177 nanocomposites were carried out by using a plate reader from Bio-Rad (Model 680; Hercules,
178 USA).

179 *2.6. Fluorometric sensing of influenza virus using the QD-peptide-AuNP sensing probe*

180 Different concentration of target virus in 20 µL was added in 180 µL solution of QD-
181 peptide-AuNP sensing probe and incubated for 3 min, thereafter fluorescence intensity was
182 measured. In the optimization process, different sized nanocomposites with different chain
183 length peptides were also applied in the identical condition. The concentration range for the
184 detection of influenza virus was 10^{-14} – 10^{-9} g mL^{-1} which was achieved in DI water. The
185 excitation wavelength for the sample solution was 450 nm and the wavelength for the
186 measurement of fluorescence intensity was in a range of 500 – 700 nm.

187

188 3. **Results and discussion**

The purpose of the present study is to construct a sensing platform for the detection of virus where the sensing parameters can be optimized according to the need of the analytes. To achieve this, a new combination of biosensor was successfully synthesized by QD-peptide-AuNP nanocomposite. After conjugating the anti-HA Ab in the peptide chain of nanocomposite, we completed the designing of sensing probe (Ab-QD-peptide-AuNP) for virus detection. Influenza virus can be detected after incubating for 3 min with our prepared sensing probe by measuring the change of fluorescence intensity (as illustrated in **Scheme 1**). As a more advanced platform from the previous studies on LSPR, the sensor gains rigid structure with tunable length which substantially reduces the noise of the background, leading to lowering the detection limit due to the covalent bonding between AuNPs and QDs through the peptide linker. We can tune the distance between CdZnSeS/ZnSeS QDs and AuNPs with different chain length of peptides, and 18 amino acids have been selected which maintain a distance of 8.5 nm approximately between two nanoparticles. Initially the CdZnSeS/ZnSeS QD-peptide-AuNP probe causes to enhance the fluorescence intensity of the QDs strongly. Due to the conjugation of primary antibody to the peptide linker between AuNPs and QDs, the sensing probe has been bound with the target virus. The antibody conjugation has been confirmed by the ELISA, shown in **Fig. S1** of Supplementary data. In the presence of target virus, the interaction between antibody and antigen creates strong steric hindrance in both sides due to two antibody anchoring side in the peptide chain. This steric hindrance restricts the LSPR between AuNPs and QDs, resulting in quenching of fluorescence. The quenching of fluorescence is directly proportional to the concentration of the target virus, confirming proficient detection ability of the proposed biosensor. To get the best suitable condition for sensing, we have varied the size, concentration of AuNPs and number of antibody binding sites keeping the QDs as a constant.

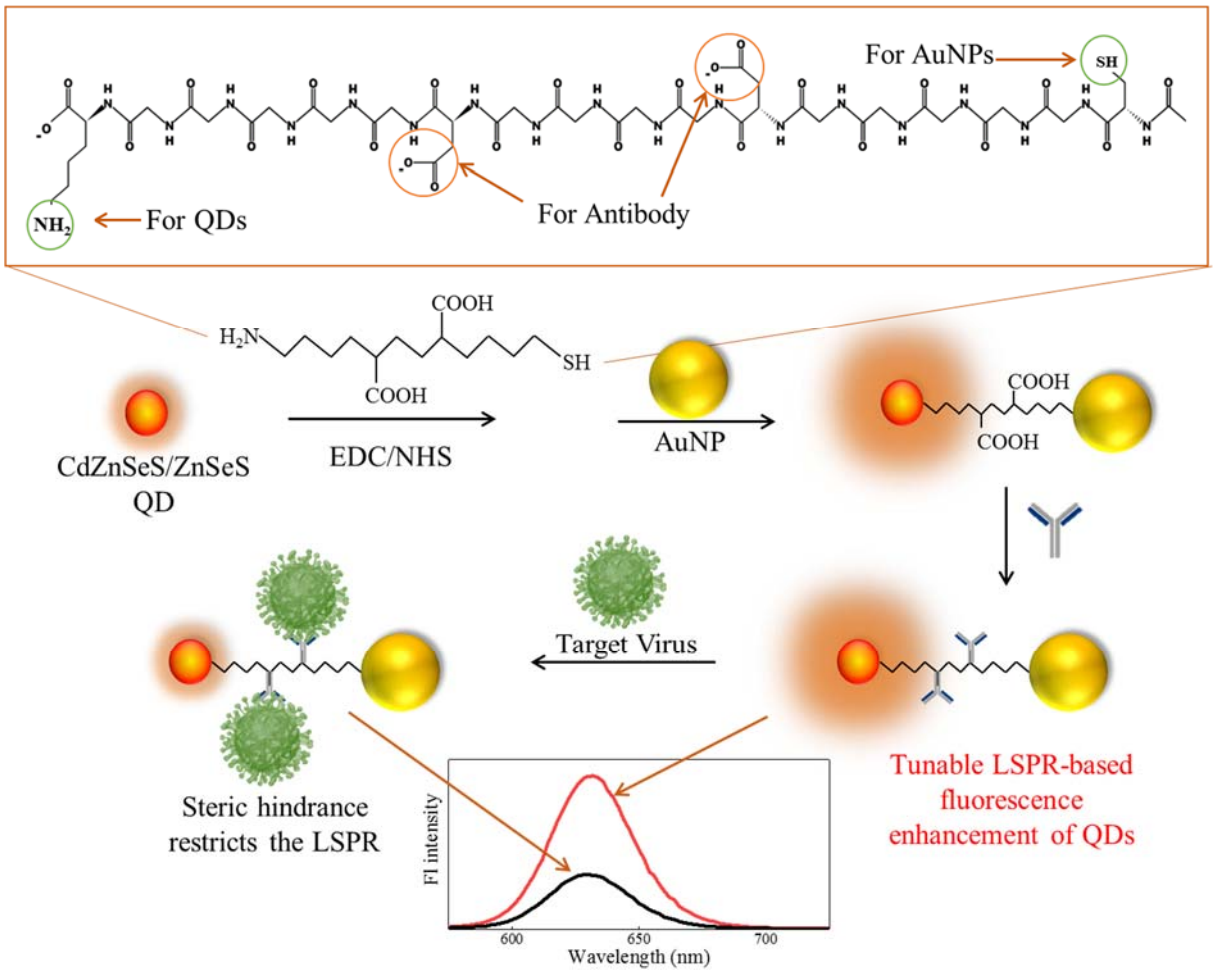

Scheme 1. Schematic diagram for the preparation of CdZnSeS/ZnSeS QD-peptide-AuNP nanocomposite and its detecting mechanism towards influenza virus. AuNPs and QDs are conjugated by peptide linker in this current work.

3.1. Characterizations of QD-peptide-AuNP sensing probe

The structure and the size distribution of individually synthesized bare CdZnSeS/ZnSeS QDs and AuNPs were examined. To obtain different sized AuNPs in the range of 10–80 nm, room temperature seed-mediated synthesis of AuNPs has been carried out to provide expanded capacity to probe [26]. After optimization, the AuNPs with 25 nm have been selected for the sensor application. The spherical shapes of AuNPs are evenly distributed in the range of 20 –

35 nm while the average particle size is 26.5 ± 0.5 nm, as shown in **Fig. 1a** and **b**. In case of bare CdZnSeS/ZnSeS QDs, the consistency of spherical shape of the particle is shown in TEM image (**Fig. 1c**). In this quenching-based study, the ultimate goal of this sensing is to reduce its fluorescence signal in the presence of virus which can restrict the LSPR between two nanoduos. Therefore, to avoid very high base fluorescence signal which is very difficult to show quenching in presence of small virus particles, a moderate quantum yield (QY) of 0.36 valued CdZnSeS/ZnSeS QDs with relatively bigger sized AuNP of 25 nm has been selected. Size distribution of the particles has been given in **Fig. 1d** in which the average particle size is shown as 4.8 ± 0.6 nm. The UV-Vis absorption and fluorescence spectra of the as synthesized CdZnSeS/ZnSeS QDs and the AuNPs are shown in **Fig. S2** of Supplementary data along with the QY measurement of the QDs which is found as 0.36. After successful preparation of the CdZnSeS/ZnSeS QD-peptide-AuNP, the nanocomposite was characterized by EDS mapped image. In **Fig. 1e**, an isolated cluster of CdZnSeS/ZnSeS QD-peptide-AuNP nanoassembly is clearly observed, the individual elements have been also observed distinctly. The nanocomposite was mapped with Au and Cd, respectively which proved the successful linkage of these two components of CdZnSeS/ZnSeS QDs and AuNPs.

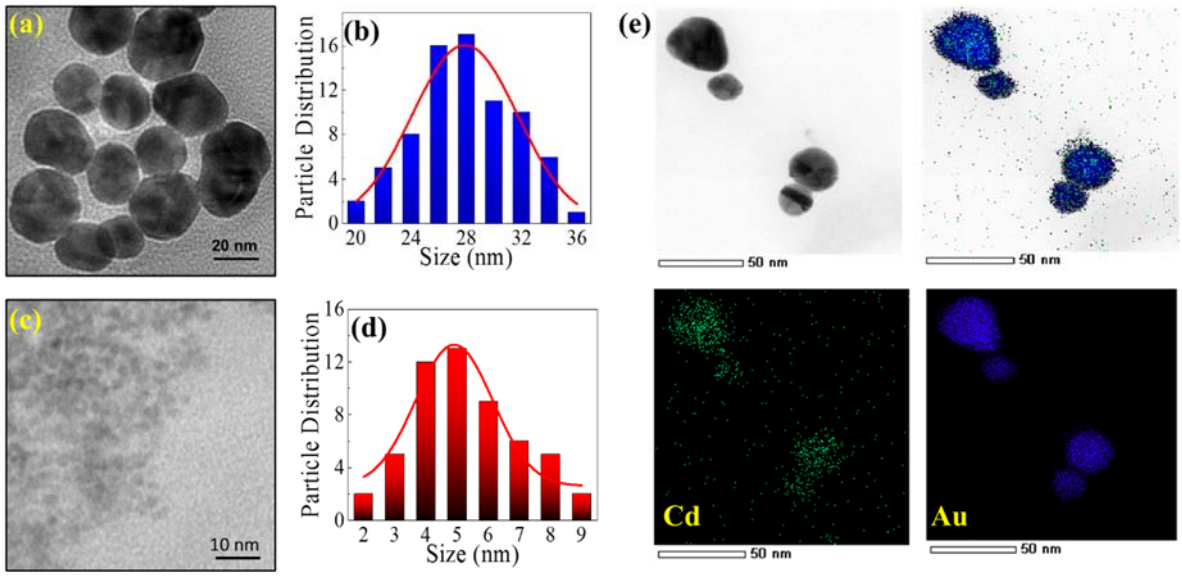

Fig. 1. TEM images (**a** and **c**) and particle size distributions (**b** and **d**) of AuNPs and CdZnSeS/ZnSeS QDs, respectively. (**e**) EDS mapping of CdZnSeS/ZnSeS QD-peptide-AuNP nanocomposites with Cd, Au and merged image.

The nanocomposites formation was further verified by hydrodynamic diameter measurement by DLS where the individual nanoparticles along with the CdZnSeS/ZnSeS QD-peptide-AuNP nanocomposites were determined and shown in **Fig. 2a**. The bare CdZnSeS/ZnSeS QDs and AuNPs shows the hydrodynamic size of 5 ± 0.5 nm and 28.4 ± 1.5 nm, respectively which are perfectly matched with their solid-state morphology, found in TEM images. However, in case of CdZnSeS/ZnSeS QD-peptide-AuNP nanocomposite, it shows the diameter of 57 ± 0.5 nm which is larger than their individual sizes, confirming the conjugated distribution. In addition, when the influenza virus was bound to sensing probe, the size of CdZnSeS/ZnSeS QD-influenza virus-peptide-AuNP nanocomposite was 172 ± 0.5 nm, suggesting the successful binding of the virus with the sensing probe. The nanocomposite formation of CdZnSeS/ZnSeS QD -peptide-AuNP from the bare CdZnSeS/ZnSeS QD-peptide and AuNP has been further verified by their XRD analysis, presented in **Fig. S3** of

Supplementary data. Similar with our previous study, the nanocomposite possesses the summation of these two crystalline nanoparticle's individual peaks in its own structure, confirming the successful formation of the CdZnSeS/ZnSeS QD -peptide-AuNP.

The successful conjugation of the nanocomposites has also confirmed by the XPS analysis. In case of survey spectrum of CdZnSeS/ZnSeS QD-peptide-AuNP in **Fig. 2b**, the induction of Au peak indicates the conjugation of AuNPs into the nanocomposites. In further analysis, the deconvoluted Au4f spectra of CdZnSeS/ZnSeS QD-peptide-AuNP have been compared with bare CdZnSeS/ZnSeS QDs in **Figs. 2c** and **d** where the introduction of strong Au peak confirms the conjugation of the nanocomposite which was completely absent for the bare CdZnSeS/ZnSeS QDs. The covalent conjugation due to linkage of peptide is further confirmed by the deconvoluted spectra of C1s. As shown in **Figs. 2e** and **f**, the intensity of carbon is drastically enhanced in case of nanocomposites compared with bare CdZnSeS/ZnSeS QDs, indicating the presence of large carbon moiety of the long peptide chain.

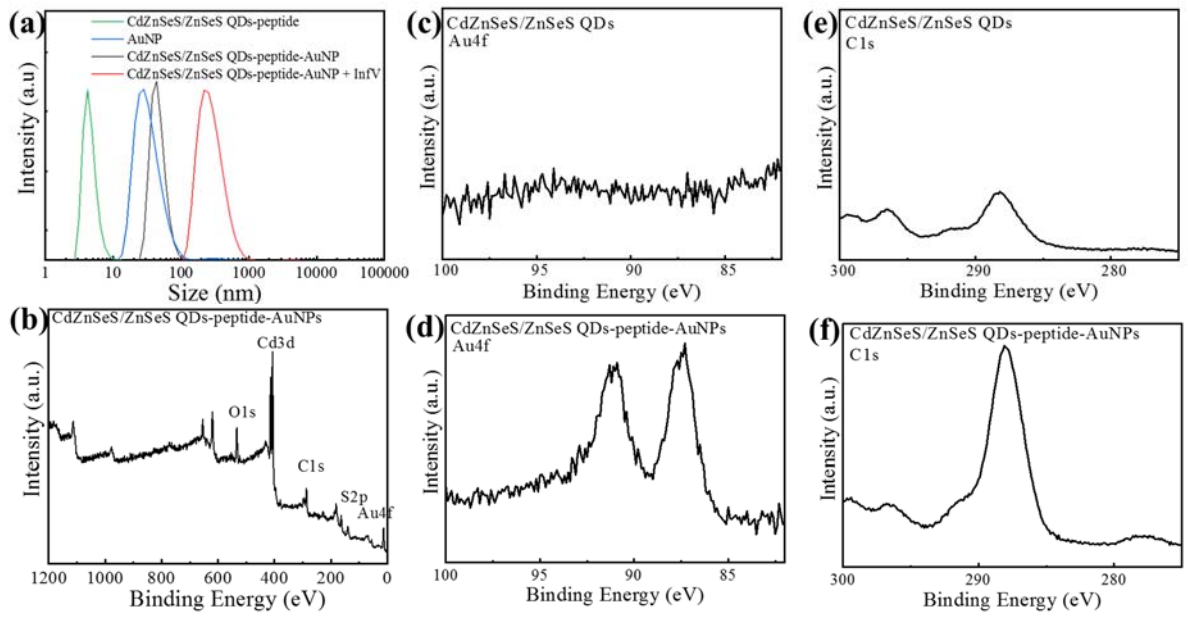

Fig. 2. (**a**) Hydrodynamic radius of CdZnSeS/ZnSeS QD-peptide-AuNP nanocomposites along with its individual components of bare AuNPs, CdZnSeS/ZnSeS QDs and Influenza virus added CdZnSeS/ZnSeS QD-peptide-AuNP, (**b**) XPS survey scan of CdZnSeS/ZnSeS QD-peptide-AuNP nanocomposite, deconvoluted Au4f spectra of (**c**) CdZnSeS/ZnSeS QDs and (**d**) CdZnSeS/ZnSeS QD-peptide-AuNP nanocomposite and deconvoluted C1s spectra of (**e**) CdZnSeS/ZnSeS QDs and (**f**) CdZnSeS/ZnSeS QD-peptide-AuNP nanocomposite.

3.2. Sensing mechanism and optimizations

The sensing mechanism is based on the LSPR-mediated fluorescent measurement of CdZnSeS/ZnSeS QDs. The CdZnSeS/ZnSeS QD-peptide-AuNP nanocomposites show the enhanced fluorescence property due to the LSPR-induced effect as the two nanoparticles are situated at a certain distance of ~8.5 nm by the linker of peptide. The probable structure has been provided in **Fig. S4** of Supplementary data. According to previous reports on LSPR, 8 – 12 nm distance between these two nanoparticles are ideal for showing enhanced fluorescence [20, 27, 28]. Due to the presence of two aspartic acid moieties in the peptide chain, two extra carboxylic acid groups can be easily conjugated with the monoclonal anti-HA antibody. According to our hypothesis, when the virus particles are added to the sensor medium, these two antibodies can bind to the virus particles by the specific antigen-antibody interaction. As the antibodies are situated in the trans position of each other, it can be anticipated that the bound viruses can produce enough steric repulsion in the process of the LSPR from AuNPs towards QDs. In spite of the reference studies from our early reports, we have also optimized the best condition for the virus sensing, varying the concentration, size of AuNPs and length of peptide chain.

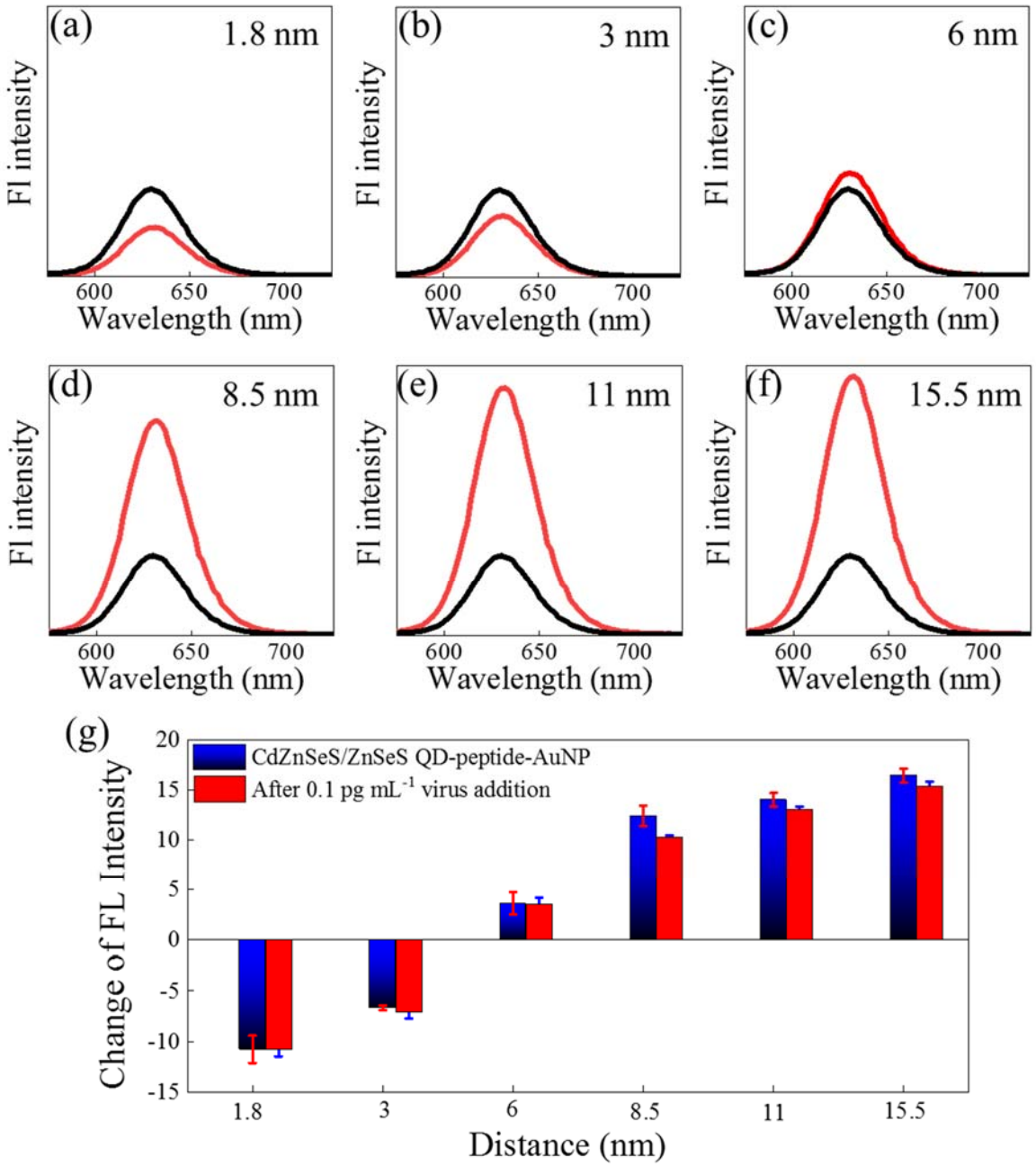

298

299 **Fig. 3.** Distance-dependent fluorescence spectra where the peptide length was varied from (**a**)
300 1.8, (**b**) 3, (**c**) 6, (**d**) 8.5, (**e**) 11 and (**f**) 15.5 nm (the black and red lines represent the
301 fluorescence of CdZnSeS/ZnSeS QD-peptide before and after conjugation with AuNPs,
302 respectively) and comparison of the change of fluorescence intensities with respect to the (**g**)
303 linked peptide chain length variation and after addition of 0.1 pg mL^{-1} Influenza virus.

304

To monitor the distance-dependent LSPR behavior, initially the 25 – 30 nm of AuNPs have been chosen for the analysis where the other parameters remains constant. As shown in the **Fig. 3a–f**, the fluorescent intensity was depending on the distance between two nanoparticles where the other parameters remain constant. In case of closely packed CdZnSeS/ZnSeS QD-peptide-AuNP nanocomposites, where the distance is only 1.8 nm, it shows prominent quenching effect. However, the quenching effect has been transformed to the fluorescence enhancement when the distance between two nanoparticles increases gradually from 1.8 to 6 nm (from 4 to 12 amino acid residues) as shown in **Fig. 3g**. The phenomenon may be explained that the quantum efficiency and the emission intensity of the QDs can be enhanced or quenched by the equilibrium of two ways of electron transfer process of non-radiative energy transfer and local field enhancement effect [28, 29]. When these two duos are in very close proximity, non-radiative energy transfer dominates, resulting the quenching of the fluorescence. With increasing the distance, the local field enhancement effect becomes significant over the non-radiative energy transfer, contributing to the enhancement of fluorescence intensity. The enhancement intensity reaches maximum at an optimal distance of about 15.5 nm and thereafter the effect from the neighboring group of metal nanoparticles became insignificant (data not shown). In case of our sensing application using this strategy, we need to choose such optimized condition, where the system has that flexibility to change its electron transfer process in addition of small number of viruses. Therefore, in case of 11 or 15.5 nm, though the system shows higher fluorescence value than the 6 or 8.5 nm, however after addition of the virus, it makes difficult to show quenching effect due to the initial high base value of the bare sensor. Keeping this in mind, it is considered that the 8.5 nm length of peptide can show the best results for the sensing study with sufficiently high amount of fluorescence, as it can offer better possibility to switch from enhancement to quenching, after addition of the sensing analytes. To get the most plausible structure of the nanocomposites, a

simplest formation of the QD-peptide-AuNP nanocomposite with 8.5 nm peptide has been evaluated for the energy minimization as given in **Fig. S5** of Supplementary data. A distance of 7.9 nm for the peptide length has been calculated from the theorical approach which is very close to the cumulative distance of the 8.5 nm of peptide chain.

3.3. Detection of influenza virus

The LSPR-induced fluorescence changes for the influenza virus detection along with its calibration curve are shown in **Fig. 4a** and **b**, respectively. Sensing signal was monitored at 630 nm for the fluorescence of the QDs. In case of CdZnSeS/ZnSeS QD-peptide, it shows 26780 fluorescence intensity which increases to 47320 after formation of the CdZnSeS/ZnSeS QD-peptide-AuNP nanocomposites, as depicted in **Fig. 4a**. After addition of increasing concentrations of influenza viruses, progressive quenching takes place without any notable peak shift. The fluorescence quenching by their initial fluorescence ($\Delta F/F_i$) are plotted against the virus concentration in **Fig. 4b** where the fluorescence quenching behavior has been found. The linearity maintains excellent up to 100 ng mL^{-1} whereas it reaches its saturation beyond that. Therefore, the corresponding linear calibration curve has been calculated from femto to 100 ng mL^{-1} concentration range and shown in **Fig. 4b**. The limit of detection (LOD) was estimated of 17.02 fg mL^{-1}, based on $L + 3\sigma$ (σ is the standard deviation of the lowest signal and L is the lowest concentration used) [30]. The advantage of this current system over other LSPR-based analysis is found in term of its rigid sensor structure by covalent attachment between two nanoparticles which developed strong fluorescence enhancement of QDs initially. Due to the rigidity of CdZnSeS/ZnSeS QD-peptide-AuNP nanostructure, the possibility of nonspecific interaction becomes negligible and the sensor cannot exhibit any significant changes until the target analytes are added, which results in very low background signal. In our

previous study, we have introduced similar type of system with a small crosslinker of 11-mercaptoundecanoic acid instead of peptide chain. However, being a small crosslinker between two nanoparticles, the precision of detection was not achieved satisfactorily as the space for the approaching virus is extremely concise. The randomness of the binding virus particles, especially in low concentration made the system little erroneous which has been overcome in case of peptide chain. To verify the stability of the sensor even after in the presence of 10 pg mL^{-1} of virus, the zeta potential has been estimated in PBS buffer (pH 7.4), as presented in **Fig. S6** of Supplementary data. The zeta potential values, found for the CdZnSeS/ZnSeS QD-peptide-AuNP nanocomposites before and after the virus addition are –19.8 and –21.2 mV, respectively which shows the appreciable stability of the nanostructure. The small increment of the negative charge may be due to the addition of the negatively charge virus particles. Consequently, the biosensor is able to show fluorescence changes significantly even after very small number of virus particles were added, resulting very low limit of detection at 17.02 fg mL^{-1}. Due to the low LOD and wide detection range, proposed biosensor shows better performances compared to other reported LSPR-based methods for influenza detection, listed in **Table 1**.

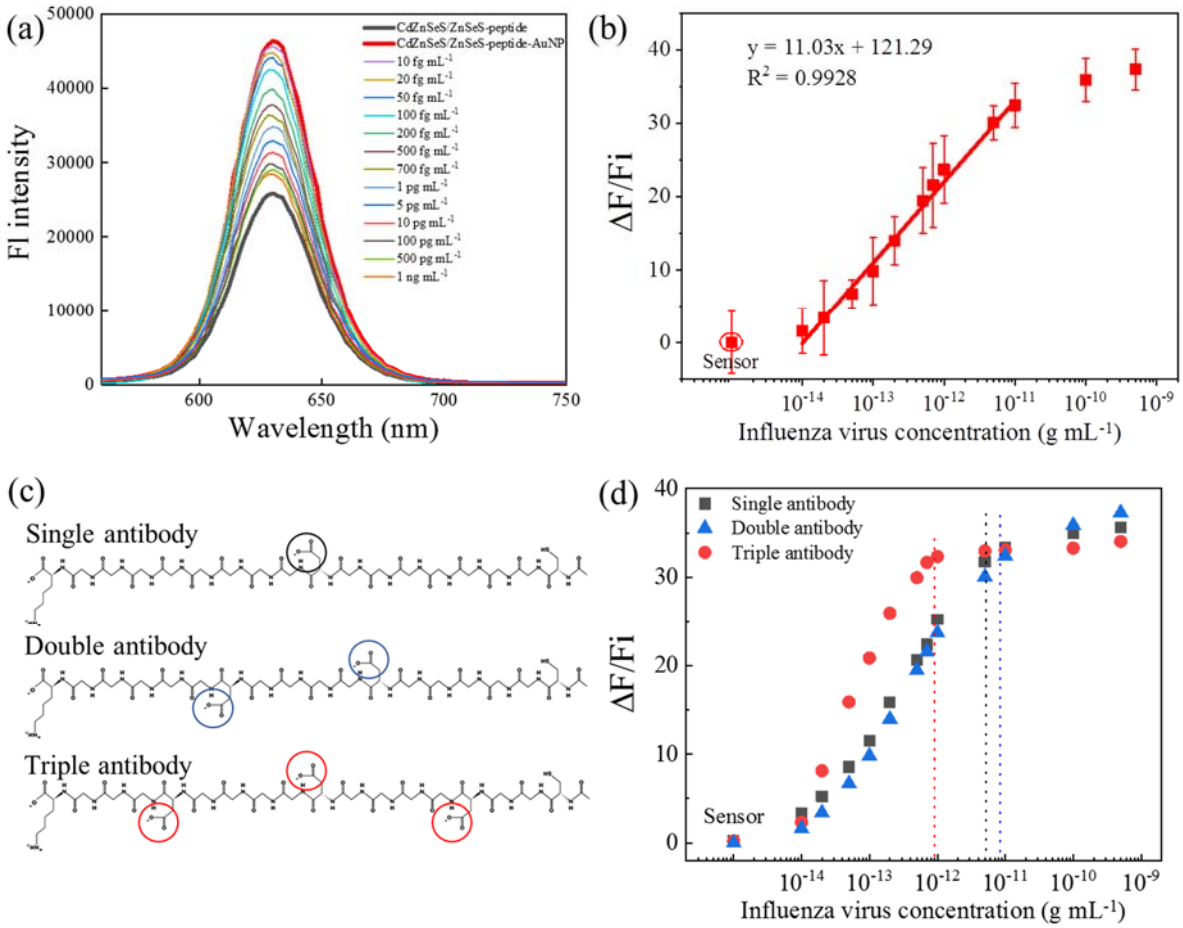

371

372 **Fig. 4.** (**a**) Fluorescence emission spectra for the detection of influenza viruses in the
373 concentration range of 10^{-14} – 10^{-9} g mL^{-1} using the LSPR-based CdZnSeS/ZnSeS QD-
374 peptide-AuNP sensing probe. (**b**) Corresponding calibration curve for detection of the
375 influenza virus with respect to the change of fluorescence intensity. Error bars denote standard
376 deviation of 3 replicate measurements. (**c**) Used peptides with different number of carboxyl
377 group. (**d**) Effect of one, double and triple antibody-conjugated sensing probe on sensing
378 performance.

379

380 As a control experiment, the interference of each individual sensor components was tested
381 with influenza viruses to verify the possible cross reactivity of the sensor materials. In this case,
382 AuNPs were physically mixed with the CdZnSeS/ZnSeS QD-peptide nanocomposite for the

detection of the target virus instead of covalently attached AuNPs. As shown in **Fig. S7** of Supplementary data, the fluorescence emission spectrum of the CdZnSeS/ZnSeS QD-peptide was unchanged after addition of AuNPs by physical mixing which indicates that the target virus cannot be detectable because without LSPR signal.

In addition, to confirm our hypothesis on the LSPR-based system, we have modified the peptide also, varying different antibody anchoring sites. Two different nanocomposites have been synthesized with peptides having one and three aspartic acid moieties (**Fig. 4c**), conjugated with the same QDs and AuNPs in a similar manner. Antibodies were conjugated to one to three aspartic acid moieties of nanocomposites to get single antibody-, double antibody- and triple antibody-conjugated sensing probe. Then these systems have been introduced to different concentration of virus solution in similar manner. As shown in **Fig. 4d**, the increasing patterns of fluorescence in case of single and double antibody-conjugated sensing probe are following almost the same trend, whereas in case of triple antibody-conjugated sensing probe, the saturation point comes earlier from 100 pg mL^{-1} to 10 pg mL^{-1}. In case of single antibody-conjugated sensing probe, the effect of steric hindrance, especially in case of small concentration, is not as significant as double antibody-conjugated one. This may be due to the fact that the single antibody-conjugated sensing probe is unable to provide enough steric influence on AuNP for successful restriction of LSPR interaction due to the one-sided vacant position even after the virus addition.

406 **Table 1:** Comparison for the detection limit of the proposed LSPR-based fluorescence
407 biosensor with other methods for the detection of influenza virus.

Detection technique	Signal type	LOD	References
LSPR-induced immunofluorescence	Fluorescence enhancement	0.03 pg mL^{-1}	[8]
Electrochemical assay	Impedance	0.9 pg μL^{-1}	[31]
Metal enhanced fluorescence	Fluorescence enhancement	1 ng mL^{-1}	[32]
Fluorescence based assay	Fluorescence enhancement	8 ng mL^{-1}	[33]
Peroxidase mimic	Colorimetric	10 pg mL^{-1}	[34]
Fluorescence emission light guide assay	Fluorescence enhancement	138 pg mL^{-1}	[35]
LSPR fiber-optic	Fluorescence enhancement	13.9 pg mL^{-1}	[36]
2D-HPLC method	HPLC-fluorescence	10^5 ng mL^{-1}	[37]
Electrochemical immunosensor	Electrodes	2.2 pg mL^{-1}	[38]
Immunochromatography assay	Colorimetric	73 ± 3.65 ng mL^{-1}	[39]
Surface plasmon resonance	Fluorescence enhancement	1.5 pg mL^{-1}	[40]
LSPR-based immunofluorescence	Fluorescence recovery	12.1 fg mL^{-1}	[20]
Tunable LSPR-based immunofluorescence	**Fluorescence quenching**	**17.02 fg mL^{-1}**	**This work**

408

409 *3.4. Selectivity and stability of the sensor*

To verify the selectivity of this proposed detection method, the detection of the target virus was compared with different kind of viruses and possible interfering agents, as shown in **Fig. 5a**. In case of most of the interferences such as sodium, potassium, phosphate ions and glycine, proline, alanine, arginine, proline etc. the matrix effects are quite low however their concentration were multiple times higher than their respective values in blood or serum. This proves that the sensitivity of the CdZnSeS/ZnSeS QD-peptide-AuNP nanocomposite is solely dependent on the antibody sites. There is no significant non-specific interaction with any other part of the biosensor. However, in case of cysteine, the interfering signal is relatively high which is almost half of the signal of low amount of virus loaded sensor response. As the sensor contain the CdSe and AuNP which have the soft interaction with the thiol group of cysteine, it can affect the sensing signal significantly, failing the selectivity of the sensor. Therefore, it is suggested that the removal of thiolated compounds like cysteine or glutathione should be carried out to obtain best result with this sensor if their concentration in sensing medium is too high. When the anti-influenza antibody loaded CdZnSeS/ZnSeS QD-peptide-AuNP sensor has been tested on different kind of viruses like Zika, NoV-LP, HEV-LP, WSSV and Dengue virus in the same concentration of 10 and 50 pg mL^{-1} or 10^4 and 10^5 copies mL^{-1}, the sensor shows almost ignorable response, indicating the sufficient specificity of our biosensor for the targeted influenza virus.

To check the sensor stability for long term use, the antibody conjugated CdZnSeS/ZnSeS QD-peptide-AuNP nanocomposites has been stored in 4°C and tested its performance with 10 and 100 pg mL^{-1} of Influenza virus in the interval of 1 week. As shown in **Fig. 5b**, the performance of the sensor has negligible effect over the first 3 weeks due to rigid structure of the sensor which proves its excellent applicability for long term usage. However, after third week, the performance degrades significantly, may be due to the instability of the antibody of the nanocomposite.

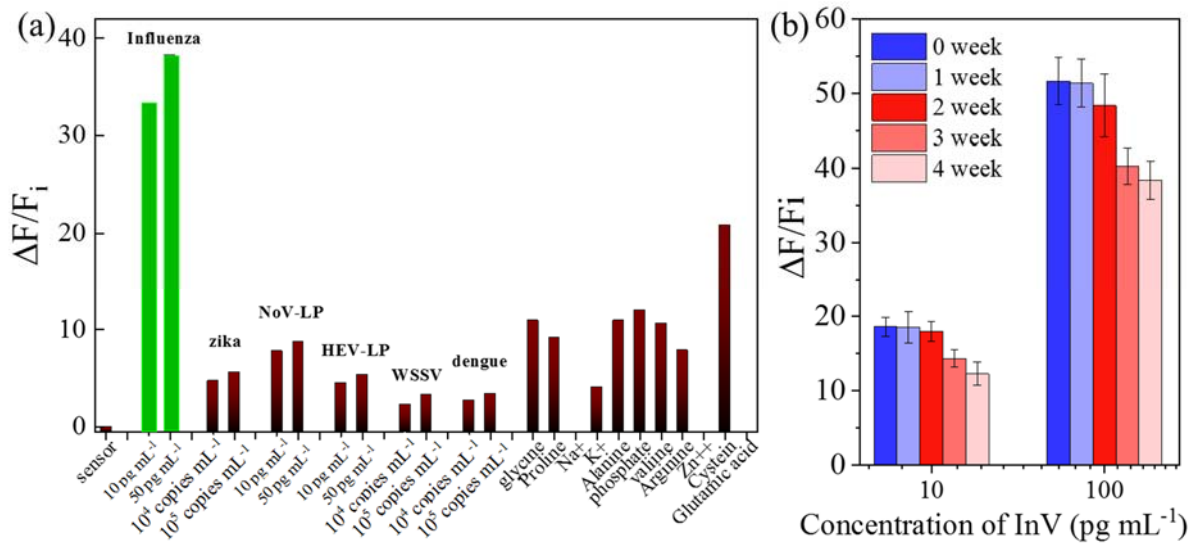

Fig. 5. (**a**) Selectivity test of the CdZnSeS/ZnSeS QD-peptide-AuNP biosensor with anti-influenza antibody. Used influenza virus, NoV-LP and HEV-LP were 10 – 50 pg mL^{-1}; Zika, WSSV and Dengue virus of 10^4 – 10^5 copies mL^{-1}. Other common interfering was tested with metal ions (0.1 mg mL^{-1}) and amino acids (2 mM mL^{-1}), (**b**) Stability of the CdZnSeS/ZnSeS QD-peptide-AuNP nanocomposites towards 10 and 100 pg mL^{-1} influenza virus over 1-month period.

3.5. Effect of virus sizes and serum matrix on sensor performances

As this sensing strategy is based on the steric influence of the viruses towards the LSPR process, the size of the target virus can be an effective parameter for analysis. To check the virus size dependency, three different sensors have been fabricated using three different antibodies of influenza, HEV-LP and WSSV separately remaining other factors unchanged. These three types of sensors have been applied to their corresponding target analytes of different sizes of influenza (100 nm), HEV-LP (30 nm) and WSSV (200 nm). As shown in **Fig.**

6a, the sizes of target viruses do not make any significant changes on the sensing performances according to their corresponding slope, indicating the uniform detection ability irrespective of target sizes. However, in case of larger size virus of WSSV, the correlation coefficient has decreased slightly which may be due to the fact that the much larger size target virus has lower possibility to bind successfully on the specific position in between the CdZnSeS/ZnSeS QD-peptide-AuNP sensor.

In the final stage of the sensing, the anti-influenza antibody-conjugated CdZnSeS/ZnSeS QD-peptide-AuNP nanocomposite has been applied on the same influenza virus in identical condition of **Fig. 4a** in serum instead of water and the performance has been compared with the calibration curve found in **Fig. 4b**. It is clear from comparison diagram of **Fig. 6b**, the performances of the sensor in 10 % serum has been degraded obviously compared to the DI water medium due to the presence of serum interferences. The large number of interferences can make some unspecific adsorption with the nanoparticles, resulting poor sensing performance. From the new slope in the serum as represented in the **Fig. 6b**, the LOD of the sensor has been calculated as 65.1 fg mL^{-1} for influenza virus. The performance of the sensor has been reduced 3 time in serum medium compared to the DI water, however, the detection limit is still satisfactory for its application for the real samples in future.

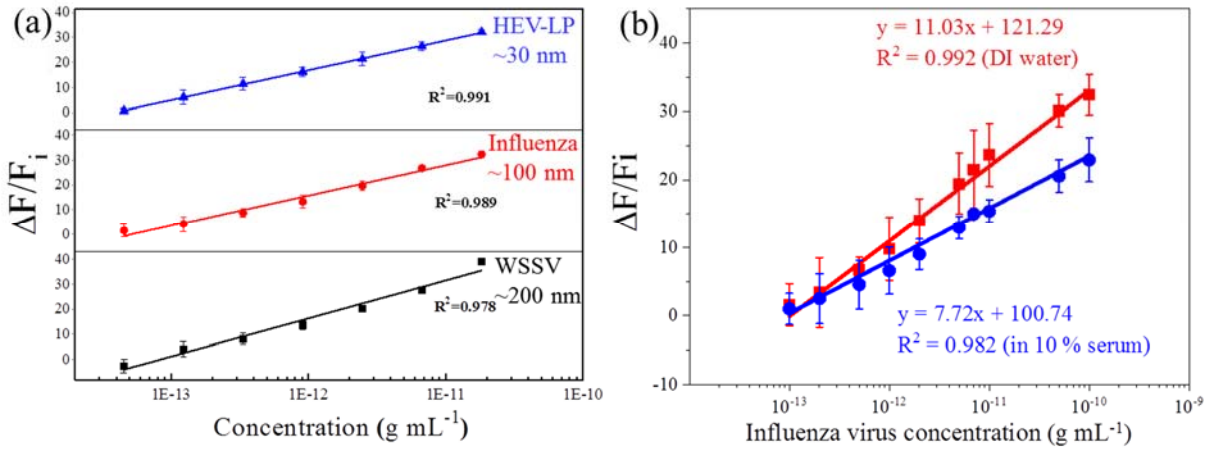

469

470 **Fig. 6.** (**a**) Comparative calibration lines for three viruses of different sizes with their
471 corresponding antibody attached CdZnSeS/ZnSeS QD-peptide-AuNP nanocomposites, (**b**)
472 Comparative calibration lines of CdZnSeS/ZnSeS QD-peptide-AuNP biosensors against the
473 influenza viruses in the range of 10^{-13} to 10^{-10} g mL^{-1} concentration in serum and DI water.

474

475 ## 4. **Conclusion**

476 In this study, a new class of nanocomposites has been synthesized using peptide chain
477 which can detect the target virus in a tunable LSPR-based fluorometric technique. The main
478 finding of this study is its detection mechanism where the fluorescence of CdZnSeS/ZnSeS
479 QDs is tuned by the adjacent AuNPs by the distance dependent LSPR. The distance has been
480 maintained by a linker of a peptide chain of 18 amino acids after functionalization in its both
481 ends. In the optimized condition, the fluorescent properties of the QDs has been enhanced
482 where the different concentration of influenza virus quenched the spectra of the QDs
483 fluorescence due to the induced steric effect. A linear range of 10^{-14} to 10^{-9} g mL^{-1} influenza
484 virus has been obtained with a detection limit of 17.02 fg mL^{-1} in water and 65.1 fg mL^{-1} in
485 serum media. On the basis of the obtained results and the detection mechanism, we hope, the
486 method of this proposed biosensor can be a good alternative for the general biomolecule

detection by changing the entrapped antibody and analytes, in the wide variety of other sensing application in future.

Declaration of competing interest

The authors declare no competing financial interest.

Acknowledgement

Authors thank Professor K. Morita of Institute of Tropical Medicine Nagasaki University, Dr, Jun Satoh of National Research Institute of Aquaculture of Japan Fisheries Research and Education Agency and Dr. Tian-Cheng Li of Department of Virology, National Institute of Infectious Diseases for providing Zika virus, WSSV and HEV-LP, respectively for the selectivity test. ADC sincerely acknowledges the Japan Society for the Promotion of Science (JSPS) for the postdoctoral fellowship (Grant No. 17F17359). This work was supported by the Bilateral Joint Research Project of the JSPS, Japan.

Appendix A. Supplementary data

Supplementary material related to this article can be found, in the online version, at doi:https://doi.org/. ELISA of CdZnSeS/ZnSeS QD-peptide-AuNP nanocomposites to confirm the antibody binding, UV-Visible characterizations of CdZnSeS/ZnSeS QDs and AuNPs and fluorescence emission spectrum of the CdZnSeS/ZnSeS QD-peptide after addition of AuNPs by physical mixing; structure of sensor.

References

509 [1] R. Monošík, M. Streďanský, E. Šturdík, Biosensors-classification, characterization and new
510 trends, Acta Chimica Slovaca, 5 (2012) 109-120.
511 [2] A.D. Chowdhury, A.B. Ganganboina, Y.-c. Tsai, H.-c. Chiu, R.-a. Doong, Multifunctional
512 GQDs-Concanavalin A@ Fe_3O_4 nanocomposites for cancer cells detection and targeted drug
513 delivery, Analytica chimica acta, 1027 (2018) 109-120.
514 [3] A.B. Ganganboina, R.-a. Doong, The biomimic oxidase activity of layered V2O5 nanozyme
515 for rapid and sensitive nanomolar detection of glutathione, Sens Actuators B, 273 (2018) 1179-
516 1186.
517 [4] A.D. Chowdhury, N. Agnihotri, A. De, M. Sarkar, Detection of positional mismatch in
518 oligonucleotide by electrochemical method, Sens Actuators B, 202 (2014) 917-923.
519 [5] Y. Liu, L. Zhang, W. Wei, H. Zhao, Z. Zhou, Y. Zhang, S. Liu, Colorimetric detection of
520 influenza A virus using antibody-functionalized gold nanoparticles, Analyst, 140 (2015) 3989-
521 3995.
522 [6] W.W. Ye, M.K. Tsang, X. Liu, M. Yang, J. Hao, Upconversion Luminescence Resonance
523 Energy Transfer (LRET)-Based Biosensor for Rapid and Ultrasensitive Detection of Avian
524 Influenza Virus H7 Subtype, Small, 10 (2014) 2390-2397.
525 [7] H. Zhang, X. Ma, S. Hu, Y. Lin, L. Guo, B. Qiu, Z. Lin, G. Chen, Highly sensitive visual
526 detection of Avian Influenza A (H7N9) virus based on the enzyme-induced metallization,
527 Biosens. Bioelectron., 79 (2016) 874-880.
528 [8] K. Takemura, O. Adegoke, N. Takahashi, T. Kato, T.-C. Li, N. Kitamoto, T. Tanaka, T.
529 Suzuki, E.Y. Park, Versatility of a localized surface plasmon resonance-based gold
530 nanoparticle-alloyed quantum dot nanobiosensor for immunofluorescence detection of viruses,
531 Biosen. Bioelectrons., 89 (2017) 998-1005.

[9] L. Shang, C. Liu, M. Watanabe, B. Chen, K. Hayashi, LSPR sensor array based on molecularly imprinted sol-gels for pattern recognition of volatile organic acids, Sens Actuators B, 249 (2017) 14-21.

[10] H. Jans, Q. Huo, Gold nanoparticle-enabled biological and chemical detection and analysis, Chem. Soc. Rev., 41 (2012) 2849-2866.

[11] J.-H. Lee, B.-C. Kim, B.-K. Oh, J.-W. Choi, Highly sensitive localized surface plasmon resonance immunosensor for label-free detection of HIV-1, Nanomed. Nanotecnol., 9 (2013) 1018-1026.

[12] A. Dutta Chowdhury, N. Agnihotri, R.-a. Doong, A. De, Label-free and nondestructive separation technique for isolation of targeted DNA from DNA–protein mixture using magnetic Au–Fe_3O_4 nanoprobes, Anal Chem, 89 (2017) 12244-12251.

[13] O. Kulakovich, N. Strekal, A. Yaroshevich, S. Maskevich, S. Gaponenko, I. Nabiev, U. Woggon, M. Artemyev, Enhanced luminescence of CdSe quantum dots on gold colloids, Nano Lett., 2 (2002) 1449-1452.

[14] S. Liu, N. Zhao, Z. Cheng, H. Liu, Amino-functionalized green fluorescent carbon dots as surface energy transfer biosensors for hyaluronidase, Nanoscale, 7 (2015) 6836-6842.

[15] A. Gowri, V. Sai, Development of LSPR based U-bent plastic optical fiber sensors, Sens Actuators B, 230 (2016) 536-543.

[16] J. Jeon, S. Uthaman, J. Lee, H. Hwang, G. Kim, P.J. Yoo, B.D. Hammock, C.S. Kim, Y.-S. Park, I.-K. Park, In-direct localized surface plasmon resonance (LSPR)-based nanosensors for highly sensitive and rapid detection of cortisol, Sens Actuators B, 266 (2018) 710-716.

[17] S.R. Ahmed, S. Oh, R. Baba, H. Zhou, S. Hwang, J. Lee, E.Y. Park, Synthesis of gold nanoparticles with buffer-dependent variations of size and morphology in biological buffers, Nanoscale Res. Lett., 11 (2016) 65.

[18] O. Adegoke, M.-W. Seo, T. Kato, S. Kawahito, E.Y. Park, An ultrasensitive SiO_2-encapsulated alloyed CdZnSeS quantum dot-molecular beacon nanobiosensor for norovirus, Biosen. Bioelectrons., 86 (2016) 135-142.

[19] A. Dutta Chowdhury, A.B. Ganganboina, F. Nasrin, K. Takemura, R.-a. Doong, D.I.S. Utomo, J. Lee, I.M. Khoris, E.Y. Park, Femtomolar detection of dengue virus DNA with serotype identification ability, Anal Chem, 90 (2018) 12464-12474.

[20] F. Nasrin, A.D. Chowdhury, K. Takemura, J. Lee, O. Adegoke, V.K. Deo, F. Abe, T. Suzuki, E.Y. Park, Single-step detection of norovirus tuning localized surface plasmon resonance-induced optical signal between gold nanoparticles and quantum dots, Biosen. Bioelectrons., 122 (2018) 16-24.

[21] T. Bedford, S. Riley, I.G. Barr, S. Broor, M. Chadha, N.J. Cox, R.S. Daniels, C.P. Gunasekaran, A.C. Hurt, A. Kelso, Global circulation patterns of seasonal influenza viruses vary with antigenic drift, Nature, 523 (2015) 217.

[22] A. Hushegyi, D. Pihíková, T. Bertok, V. Adam, R. Kizek, J. Tkac, Ultrasensitive detection of influenza viruses with a glycan-based impedimetric biosensor, Biosens. Bioelectron., 79 (2016) 644-649.

[23] M. Peiris, K. Yuen, C. Leung, K. Chan, P. Ip, R. Lai, W. Orr, K. Shortridge, Human infection with influenza H9N2, Lancet, 354 (1999) 916-917.

[24] S.R. Ahmed, J. Kim, T. Suzuki, J. Lee, E.Y. Park, Enhanced catalytic activity of gold nanoparticle-carbon nanotube hybrids for influenza virus detection, Biosen. Bioelectrons., 85 (2016) 503-508.

[25] O. Adegoke, M.-W. Seo, T. Kato, S. Kawahito, E.Y. Park, Gradient band gap engineered alloyed quaternary/ternary CdZnSeS/ZnSeS quantum dots: an ultrasensitive fluorescence reporter in a conjugated molecular beacon system for the biosensing of influenza virus RNA, Journal of Materials Chemistry B, 4 (2016) 1489-1498.

581 [26] W. Leng, P. Pati, P.J. Vikesland, Room temperature seed mediated growth of gold
582 nanoparticles: mechanistic investigations and life cycle assesment, Environmental Science:
583 Nano, 2 (2015) 440-453.
584 [27] M.-X. Li, W. Zhao, G.-S. Qian, Q.-M. Feng, J.-J. Xu, H.-Y. Chen, Distance mediated
585 electrochemiluminescence enhancement of CdS thin films induced by the plasmon coupling of
586 gold nanoparticle dimers, Chem. Commun., 52 (2016) 14230-14233.
587 [28] A.L. Feng, M.L. You, L. Tian, S. Singamaneni, M. Liu, Z. Duan, T.J. Lu, F. Xu, M. Lin,
588 Distance-dependent plasmon-enhanced fluorescence of upconversion nanoparticles using
589 polyelectrolyte multilayers as tunable spacers, Sci Rep, 5 (2015) 7779.
590 [29] Q. Hao, D. Du, C. Wang, W. Li, H. Huang, J. Li, T. Qiu, P.K. Chu, Plasmon-induced
591 broadband fluorescence enhancement on Al-Ag bimetallic substrates, Sci. Rep., 4 (2014) 6014.
592 [30] A. Shrivastava, V.B. Gupta, Methods for the determination of limit of detection and limit
593 of quantitation of the analytical methods, Chron. Young Sci., 2 (2011) 21.
594 [31] C. Bai, Z. Lu, H. Jiang, Z. Yang, X. Liu, H. Ding, H. Li, J. Dong, A. Huang, T. Fang,
595 Aptamer selection and application in multivalent binding-based electrical impedance detection
596 of inactivated H1N1 virus, Biosens. Bioelectron., 110 (2018) 162-167.
597 [32] S.R. Ahmed, M.A. Hossain, J.Y. Park, S.-H. Kim, D. Lee, T. Suzuki, J. Lee, E.Y. Park,
598 Metal enhanced fluorescence on nanoporous gold leaf-based assay platform for virus detection,
599 Biosen. Bioelectrons., 58 (2014) 33-39.
600 [33] Y.-T. Tseng, C.-H. Wang, C.-P. Chang, G.-B. Lee, Integrated microfluidic system for
601 rapid detection of influenza H1N1 virus using a sandwich-based aptamer assay, Biosens.
602 Bioelectron., 82 (2016) 105-111.
603 [34] S.R. Ahmed, J. Kim, T. Suzuki, J. Lee, E.Y. Park, Detection of influenza virus using
604 peroxidase-mimic of gold nanoparticles, Biotechnol. Bioeng., 113 (2016) 2298-2303.

605 [35] S. Oh, J. Kim, V.T. Tran, D.K. Lee, S.R. Ahmed, J.C. Hong, J. Lee, E.Y. Park, J. Lee,
606 Magnetic nanozyme-linked immunosorbent assay for ultrasensitive influenza A virus detection,
607 ACS Appl. Mater. Interfaces, 10 (2018) 12534-12543.
608 [36] Y.-F. Chang, S.-F. Wang, J.C. Huang, L.-C. Su, L. Yao, Y.-C. Li, S.-C. Wu, Y.-M.A.
609 Chen, J.-P. Hsieh, C. Chou, Detection of swine-origin influenza A (H1N1) viruses using a
610 localized surface plasmon coupled fluorescence fiber-optic biosensor, Biosens. Bioelectron.,
611 26 (2010) 1068-1073.
612 [37] V. García-Cañas, B. Lorbetskie, D. Bertrand, T.D. Cyr, M. Girard, Selective and
613 quantitative detection of influenza virus proteins in commercial vaccines using two-
614 dimensional high-performance liquid chromatography and fluorescence detection, Anal Chem.,
615 79 (2007) 3164-3172.
616 [38] U. Jarocka, R. Sawicka, A. Góra-Sochacka, A. Sirko, W. Zagórski-Ostoja, J. Radecki, H.
617 Radecka, An immunosensor based on antibody binding fragments attached to gold
618 nanoparticles for the detection of peptides derived from avian influenza hemagglutinin H5,
619 Sensors, 14 (2014) 15714-15728.
620 [39] G.-C. Lee, E.-S. Jeon, W.-S. Kim, D.T. Le, J.-H. Yoo, C.-K. Chong, Evaluation of a rapid
621 diagnostic test, NanoSign® Influenza A/B Antigen, for detection of the 2009 pandemic
622 influenza A/H1N1 viruses, Virol. J., 7 (2010) 244.
623 [40] L.-C. Su, C.-M. Chang, Y.-L. Tseng, Y.-F. Chang, Y.-C. Li, Y.-S. Chang, C. Chou, Rapid
624 and highly sensitive method for influenza A (H1N1) virus detection, Anal Chem., 84 (2012)
625 3914-3920.

626

Supplementary data

Fluorometric virus detection platform using quantum dots-gold nanocomposites optimizing the linker length variation

Fahmida Nasrin,[a,†] Ankan Dutta Chowdhury,[b,†] Kenshin Takemura,[a] Ikko Kozaki,[c] Hiroyuki Honda,[c] Oluwasesan Adegoke[b,‡], Enoch Y. Park[*,a,b]

[a]*Laboratory of Biotechnology, Graduate School of Science and Technology, Shizuoka University, 836 Ohya, Suruga-ku, Shizuoka 422-8529, Japan*

[b]*Laboratory of Biotechnology, Research Institute of Green Science and Technology, Shizuoka University, 836 Ohya, Suruga-ku, Shizuoka 422-8529, Japan*

[c]*Department of Biomolecular Engineering, Graduate School of Engineering, Nagoya University, Furo-cho, Chikusa-ku, Nagoya 464-8603, Japan*

[†] Equally contributed.

[‡] Present address: Leverhulme Research Centre for Forensic Science, University of Dundee, UK

E-mails:
fahmida.nasrin.17@shizuoka.ac.jp (FN)
ankan.dutta.chowdhury@shizuoka.ac.jp (ADC)
takemura.kenshin.16@shizuoka.ac.jp (KT)
kozaki.ikkou@b.mbox.nagoya-u.ac.jp (IK)
honda@chembio.nagoya-u.ac.jp (HH)
o.adegoke@dundee.ac.uk (OA)
park.enoch@shizuoka.ac.jp (EYP)

---

[*]Corresponding Author at Research Institute of Green Science and Technology, Shizuoka University, 836 Ohya Suruga-ku, Shizuoka 422-8529, Japan.
E-mail addresses: park.enoch@shizuoka.ac.jp (E.Y. Park)

Table S1. Structure of different length peptides used in this work:

1. AcO-CGGGGGGGGGGDGGGGGGGGGGDGGGGGGGGGGK (34) (~15.5 nm)

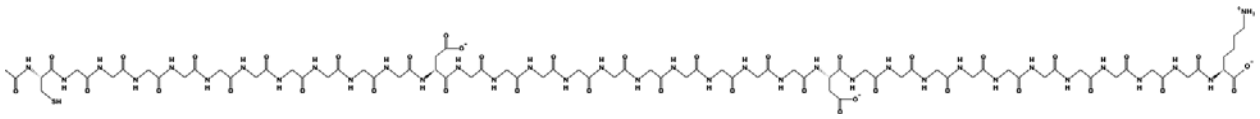

2. AcO-CGGGGGGGDGGGGGGDGGGGGGGK (24) (~11 nm)

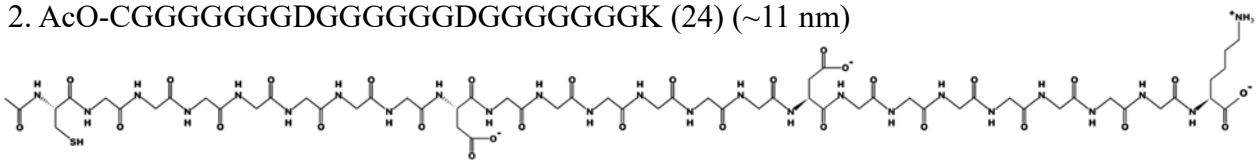

3. AcO-CGGGGGDGGGGDGGGGGK (18) (~8.5 nm)

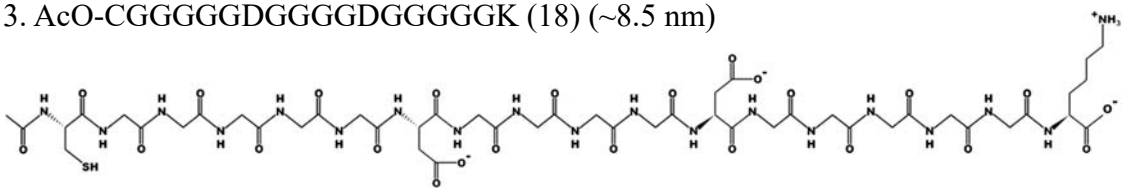

4. AcO-CGGGDGGDGGGK (12) (~6nm)

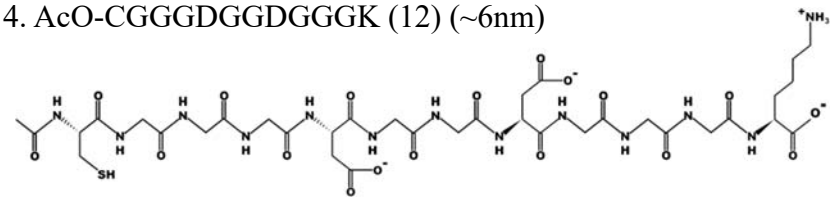

5. AcO-CGDDGK (6) (~3 nm)

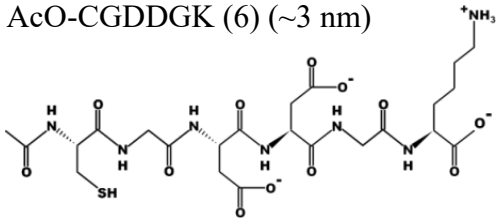

6. AcO-CDDK (4) (~1.8 nm)

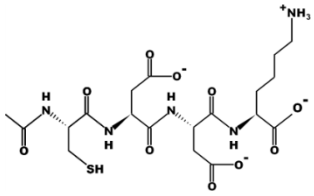

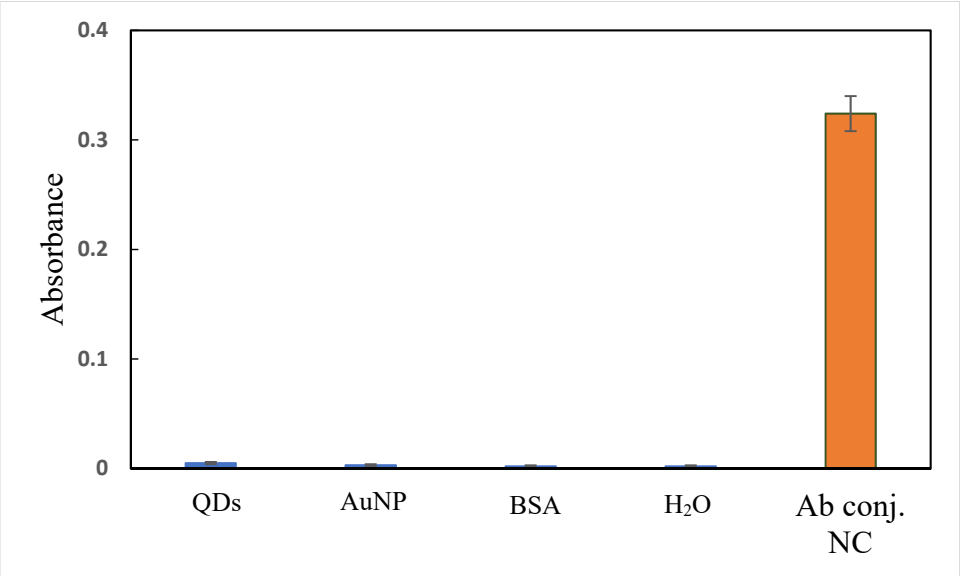

Fig. S1. ELISA of the antibody-conjugated nanocomposites along with negative controls.

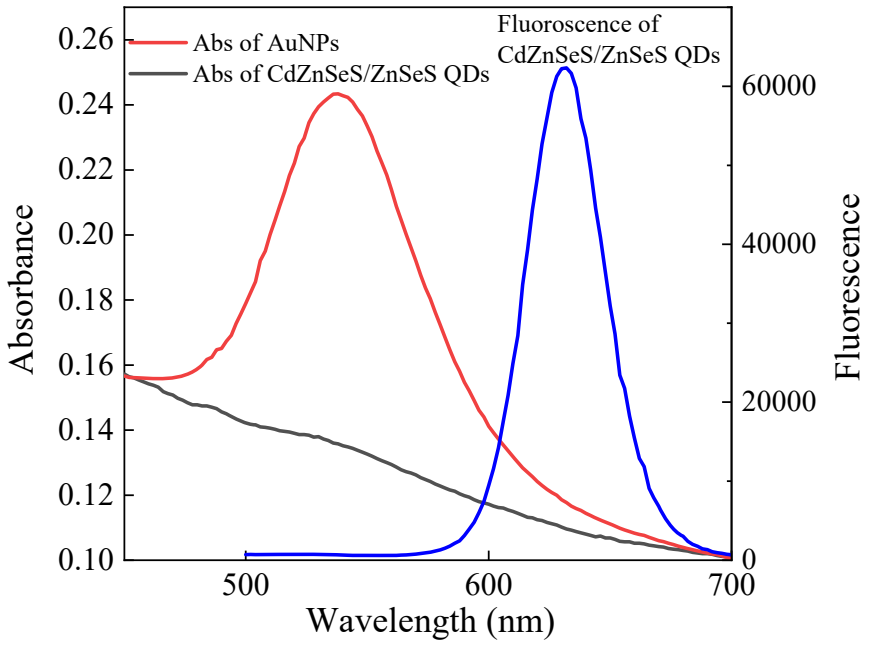

Fig. S2A. UV-Visible spectra of bare AuNPs and after formation of CdZnSeS/ZnSeS QD-peptide-AuNP nanocomposite where the SPR peak of Au is presented in both cases and the fluorescence spectra of bare CdZnSeS/ZnSeS QDs.

Measurement of quantum yield (QY) of CdZnSeS/ZnSeS QD:

The quantum yield (QY) of QDs was measured and calculated by the comparative fluorescence method using fluorescein as a standard fluorophore ($\Phi = 0.79$). Five different concentrations of fluorescein and QD solutions were prepared using deionized water. Then, the absorbance as well as the corresponding fluorescence curve of each solution was recorded and calculated from the following equation:

$$QY = Q_R\,[m/m_R][n^2/n_R^2]$$

where m is the slope of the line obtained from two calibration lines, n is the refractive index of solvent and subscript R refers to the reference fluorophore of known QY.

$$QY_{CdZnSeS/ZnSeS} = 0.79 \times 6.6/14.4 = 0.36$$

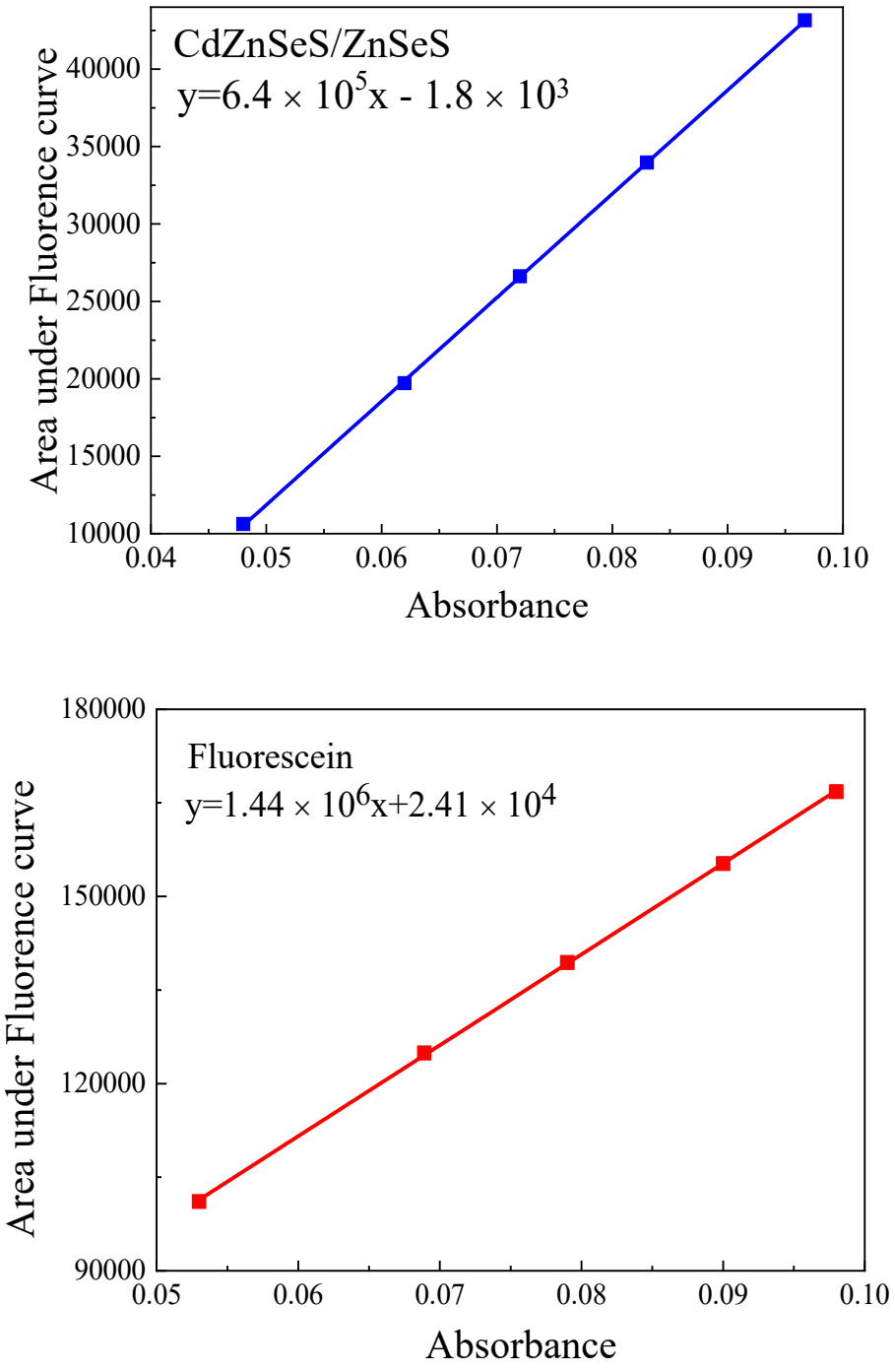

Fig. S2B. The linear relationship between fluorescence curve areas and corresponding optical density from absorbance. (a) CdZnSeS/ZnSeS QDs and (b) fluorescein.

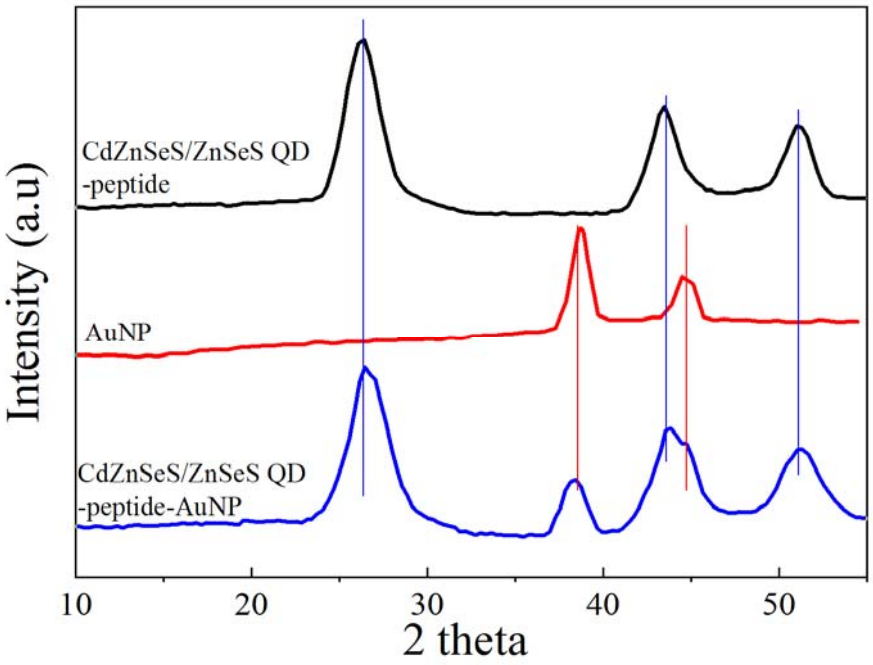

Fig. S3. XRD patterns of bare AuNP, CdZnSeS/ZnSeS QDs and CdZnSeS/ZnSeS QD -peptide-AuNP nanocomposites.

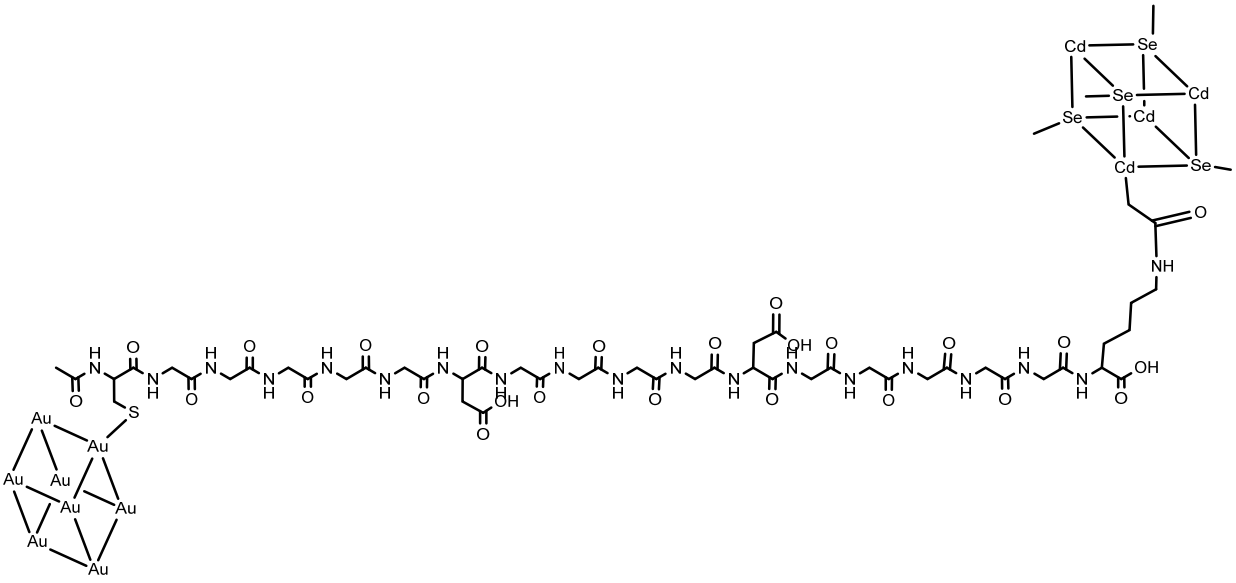

Fig. S4. Probable structure of CdZnSeS/ZnSeS QD-peptide-AuNP nanocomposite.

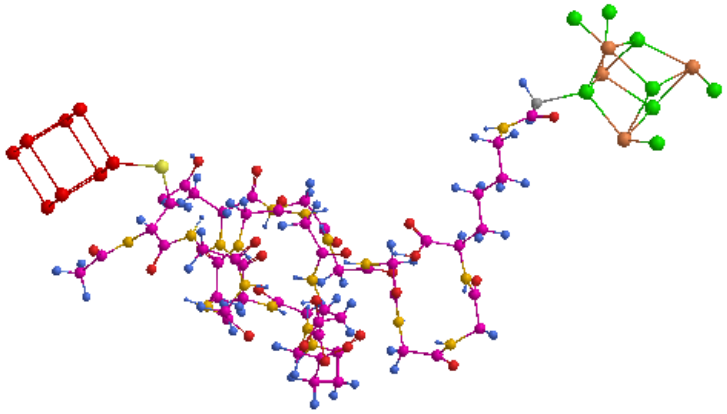

Fig. S5. Simulated structure of the CdZnSeS/ZnSeS QD -peptide-AuNP nanocomposites with the peptide chain length of 8.5 nm.

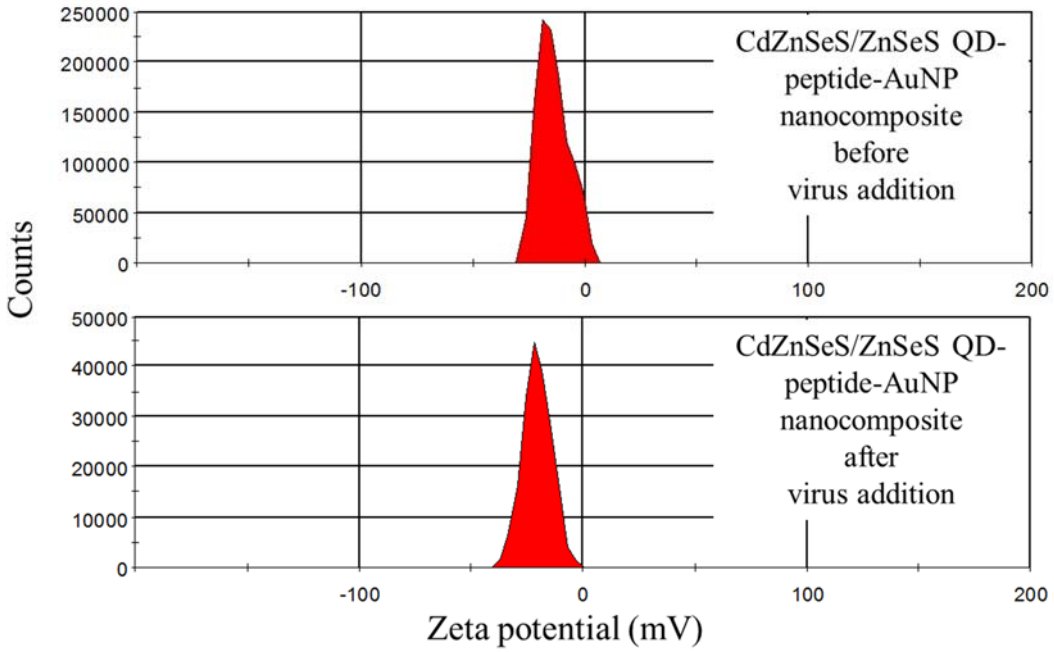

Fig. S6. Zeta potential measurement of the CdZnSeS/ZnSeS QD-peptide-AuNP nanocomposites before and after the addition of 10 pg mL^{-1} virus.

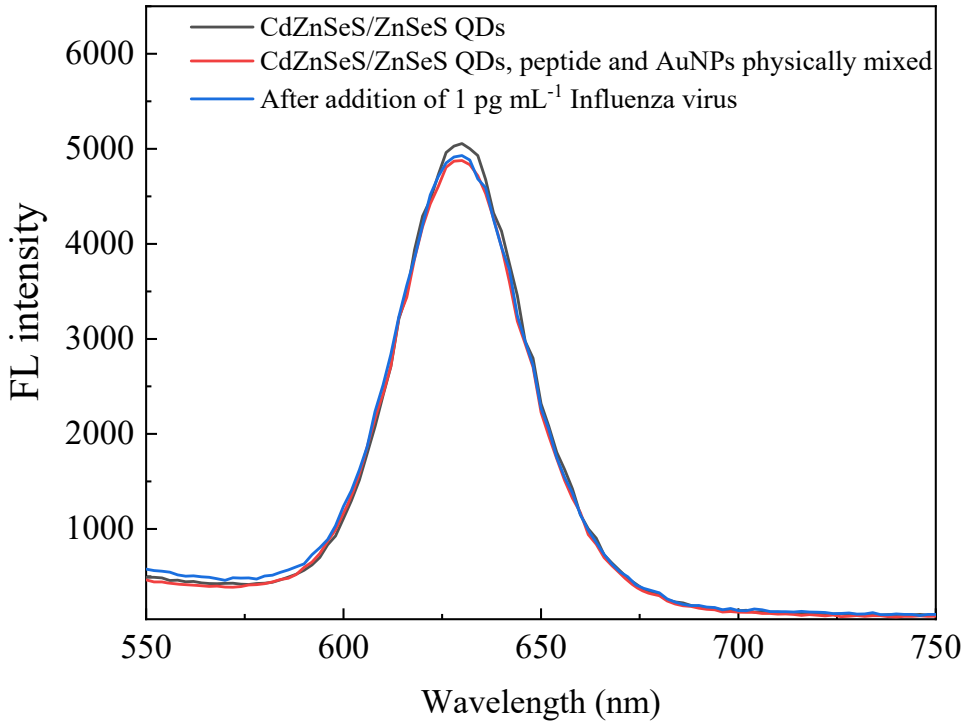

Fig. S7. The fluorescence of the sensor is unaffected when all the sensor components are only physically mixed.